Particle Size Calibration Testing in the NASA Propulsion Systems Laboratory

Michael C. King
Glenn Research Center, Cleveland, Ohio

Julien Manin
Artium Technologies, Inc., Sunnyvale, California

Judith F. Van Zante
Glenn Research Center, Cleveland, Ohio

Emily N. Timko
Jacobs Technology, Inc., Cleveland, Ohio

Peter M. Struk
Glenn Research Center, Cleveland, Ohio

April 2019

NASA STI Program . . . in Profile

Since its founding, NASA has been dedicated to the advancement of aeronautics and space science. The NASA Scientific and Technical Information (STI) Program plays a key part in helping NASA maintain this important role.

The NASA STI Program operates under the auspices of the Agency Chief Information Officer. It collects, organizes, provides for archiving, and disseminates NASA's STI. The NASA STI Program provides access to the NASA Technical Report Server—Registered (NTRS Reg) and NASA Technical Report Server—Public (NTRS) thus providing one of the largest collections of aeronautical and space science STI in the world. Results are published in both non-NASA channels and by NASA in the NASA STI Report Series, which includes the following report types:

- TECHNICAL PUBLICATION. Reports of completed research or a major significant phase of research that present the results of NASA programs and include extensive data or theoretical analysis. Includes compilations of significant scientific and technical data and information deemed to be of continuing reference value. NASA counter-part of peer-reviewed formal professional papers, but has less stringent limitations on manuscript length and extent of graphic presentations.

- TECHNICAL MEMORANDUM. Scientific and technical findings that are preliminary or of specialized interest, e.g., "quick-release" reports, working papers, and bibliographies that contain minimal annotation. Does not contain extensive analysis.

- CONTRACTOR REPORT. Scientific and technical findings by NASA-sponsored contractors and grantees.

- CONFERENCE PUBLICATION. Collected papers from scientific and technical conferences, symposia, seminars, or other meetings sponsored or co-sponsored by NASA.

- SPECIAL PUBLICATION. Scientific, technical, or historical information from NASA programs, projects, and missions, often concerned with subjects having substantial public interest.

- TECHNICAL TRANSLATION. English-language translations of foreign scientific and technical material pertinent to NASA's mission.

For more information about the NASA STI program, see the following:

- Access the NASA STI program home page at http://www.sti.nasa.gov

- E-mail your question to help@sti.nasa.gov

- Fax your question to the NASA STI Information Desk at 757-864-6500

- Telephone the NASA STI Information Desk at 757-864-9658

- Write to:
  NASA STI Program
  Mail Stop 148
  NASA Langley Research Center
  Hampton, VA 23681-2199

Particle Size Calibration Testing in the NASA Propulsion Systems Laboratory

Michael C. King
Glenn Research Center, Cleveland, Ohio

Julien Manin
Artium Technologies, Inc., Sunnyvale, California

Judith F. Van Zante
Glenn Research Center, Cleveland, Ohio

Emily N. Timko
Jacobs Technology, Inc., Cleveland, Ohio

Peter M. Struk
Glenn Research Center, Cleveland, Ohio

Acknowledgments

Level of Review: This material has been technically reviewed by technical management.

Particle Size Calibration Testing in the NASA Propulsion Systems Laboratory

Michael C. King
National Aeronautics and Space Administration
Glenn Research Center
Cleveland, Ohio 44135

Julien Manin
Artium Technologies, Inc.
Sunnyvale, California 94085

Judith F. Van Zante
National Aeronautics and Space Administration
Glenn Research Center
Cleveland, Ohio 44135

Emily N. Timko
Jacobs Technology, Inc.
Cleveland, Ohio 44135

Peter M. Struk
National Aeronautics and Space Administration
Glenn Research Center
Cleveland, Ohio 44135

Abstract

The particle size characterization portion of the 2017 Propulsion Systems Laboratory Cloud Calibration is described. The work focuses on characterizing the particle size distribution of the icing cloud as a function of simulated atmospheric conditions. These results will aid in upcoming ice crystal and supercooled liquid icing tests in Propulsion Systems Laboratory (PSL). Measurements acquired with the Phase Doppler Interferometer and High Speed Imaging instruments are presented. Experimental results indicate that the particle size distribution is primarily a function nozzle air and water pressures, and that air speed is not a significant effect for ice crystal clouds in PSL and both thermodynamic conditions and air speed are not significant effects for supercooled liquid water clouds in PSL.

Nomenclature

Δp	Nozzle Water-Air Differential Pressure
$d_{v0.10}$	10th Percentile Cumulative Volume Diameter
$d_{v0.25}$	25th Percentile Cumulative Volume Diameter
$d_{v0.50}$	50th Percentile Cumulative Volume Diameter, Median Volumetric Diameter
$d_{v0.75}$	25th Percentile Cumulative Volume Diameter
$d_{v0.90}$	90th Percentile Cumulative Volume Diameter
HSI	High Speed Imaging
ICI	Ice Crystal Icing
IKP2	Isokinetic Probe
LWC	Liquid Water Content

MW	Multi-Element Probe (commonly known as the "Multi-Wire")
ND	Number Density
p_{AIR}	Nozzle Air Pressure
PDI	Phase Doppler Interferometer
ϕ_{PL}	Plenum Relative Humidity Upstream of the Spray Bars
p_{PL}	Plenum Pressure
p_{SI}	Station 1 Pressure
PSL	Propulsion Systems Laboratory
PSD	Particle Size Distribution
T_{PL}	Plenum Temperature
T_{WB}	Plenum Wet Bulb Temperature (based on conditions in the Plenum)
TWC	Total Water Content
u_{SI}	Station 1 Air Speed

Introduction

The ingestion of ice crystals into jet engines has been attributed to uncommanded jet engine power loss events during flight (Refs. 1 to 5), and has become a significant focus for research in the atmospheric icing community. As a result, NASA has been conducting ice crystal icing (ICI) studies in the NASA Propulsion Systems Laboratory (PSL) to advance the community's understanding of the fundamental physics behind this aviation safety hazard (Refs. 6 to 8). The unique nature of ICI conditions has stimulated the development of newer instrumentation to measure such conditions. The Artium Technologies, Inc. Phase Doppler Interferometer (PDI) and High Speed Imaging (HSI) instruments are two such examples that have been further developed as a result of the community's interest in ICI and funding support through NASA's Small Business Innovative Research (SBIR) program (Ref. 9).

This paper presents particle measurements acquired using the PDI and HSI instruments in the PSL during the Could Calibration Test conducted in September of 2017. One objective of this test campaign was to characterize the PSD of the icing cloud as a function of simulated atmospheric conditions, including pressure, temperature, humidity and speed. The results presented herein examine the data acquired from the Modular PDI (PDI-MOD), the Modular HSI (HSI-MOD), and the Dual Range Flight Probe HSI (HSI-FPDR) during the test. This combination of diagnostics made it possible to evaluate the effects of simulated atmospheric conditions in PSL on the particle size distribution (PSD).

Experimental Description

The goal of the 2017 PSL Cloud Calibration Test was to prepare for an upcoming research engine test. Complete descriptions of the facility are available in References 2, 5, and 8. In addition to the Artium Technologies, Inc. PDI and HSI, several other instruments were used to characterize the conditions. These included systems from Science Engineering Associates, Inc. (SEA) and NASA. The SEA Multi-Element Probe, commonly referred to as the Multi-wire (MW), and the NASA Isokinetic Probe (Ref. 10) (IKP2), both developed by SEA under a NASA contract, were used to measure the water content. Cloud uniformity was measured using the NASA Tomography System (Ref. 11), and air temperature and humidity were measured by a rearward facing, forced ingestion probe (Ref. 12). Unlike previous tests (Ref. 9), no other instruments besides the Artium Technologies, Inc. systems were used to measure the PSD during the test. While some of the results from the water content are presented in this document for comparison purposes, the water content and cloud uniformity characterization are primarily covered in Reference 13, and the results from the temperature and humidity characterization are primarily covered in Reference 14.

Phase Doppler Interferometer and High Speed Imaging Instruments

The PDI is a single particle counter using a flux sampling technique. The physical principles underlying the PDI have been well documented in numerous publications, including Reference 15. The PDI system splits a laser beam and focuses the two resulting coherent beams to a common point in space, creating an interrogation volume and generating a local interference fringe pattern. Particles passing through this volume will scatter the light, creating a Doppler burst signal as they pass the interference fringe pattern. The Artium Technologies, Inc. PDI measures this Doppler burst with three detectors at separate spatial locations. The resulting phase shift of the Doppler burst signals allows measurement of the spacing of the interference fringe pattern, which is used to determine particle size. Using three detectors provides a means to avoid phase ambiguity when the phase cycles past 360°, and also provides redundant measurements that are used to validate the signals, offering an indication as to whether the particles are quasi-spherical or irregular-shaped ice particles. The system can size spherical and quasi-spherical particles, but irregularly-shaped or faceted and partially melted particles will not follow the calibrated phase shift-size relationship, which provides an avenue for particle material phase and morphology discrimination (Ref. 9).

The HSI is another particle sizing instrument that uses a spatial sampling technique. The HSI acquires high-resolution images of the particle field passing through the sample volume. This volume is created by focusing several laser beams on a common spatial point, illuminating particles for image capture by a CMOS camera with long range optics, which is recording at a fixed rate. The rate for the HSI-MOD is 60 Hz, and the rate for the HSI-FPDR is 300 Hz. For both systems, the lasers are simultaneously pulsed with a pulse duration on the nanosecond time-scale, setting the effective exposure times, and avoiding motion blurring of the imaged particles. With knowledge of the system resolution, the system can size spherical and irregularly shaped particles, and quantitative assessments of particle morphology can be made, allowing for potential identification of glaciated particles (Ref. 9). The digital resolutions for both the HSI-MOD and Channel 1 (Ch1) of the HSI-FPDR during the test was set to 3.73 μm/pixel, but the image size for the HSI-MOD was approximately eight times larger than the HSI-FPDR image of 640 by 480 pix^2 at 1920 by 1200 pix^2. Due to a low sample volume rate, as defined by the field of view, depth of field and frame-rate, the HSI must acquire data for a longer duration to obtain sufficient statistics for the upper end of the size spectrum

The Artium PDI-MOD and HSI-MOD used during the test were non-intrusive, while the HSI-FPDR was situated in the flow. Figure 1 shows the experimental setup for the PSD phase of the PSL Cloud Calibration Test. The PDI-MOD, the HSI-MOD, and the HSI-FPDR, which are labeled in Figure 1, are positioned such that each instruments' interrogation volumes were approximately on the centerline. The interrogation volumes for the PDI-MOD and HSI-MOD were a couple centimeters forward of the HSI-FPDR probe arms. Due to space limitations, all three instruments were situated approximately 60 cm downstream of the exit plane of the duct.

Test Matrix

PSD data was acquired with the PDI-MOD, HSI-MOD and HSI-FPDR for 58 different conditions, which have been summarized in Tables 1 and 2. Table 1 summarizes the test conditions for ice crystal clouds, and Table 2 summarizes the test conditions for the supercooled liquid water clouds. The test conditions conducted during this effort included several conditions sweeps, but did not include repeated conditions. Of particular note are the nozzle water-air differential pressure, Δp, sweeps. In Table 1, these include the p_{AIR} = 20 psi, T_{WB} > 0 °F series, given by Escort Numbers 225 through 232, the p_{AIR} = 30 psi, T_{WB} > 0 °F series, given by Escort Numbers 233 through 236, and the p_{AIR} = 20 psi, T_{WB} < 0 °F series, given by Escort Numbers 248 through 252. In Table 2, the Δp sweeps include the p_{AIR} = 15 psi series, given by Escort Numbers 265 through 267, and the p_{AIR} = 20 psi series, given by Escort Numbers 268 through 271.

Processing and Results

The following subsections present the experimental results with a description of how the data was processed. Each subsection includes a table providing the water content and cumulative volume distribution values derived from the Artium instruments.

Ice Crystal Test Conditions

As mentioned in the previous section, the PDI is capable of sizing spherical and quasi-spherical particles, but irregularly shaped or faceted and partially melted particles will not follow the calibrated phase shift-size relationship, hindering the ability to size these particles with the PDI. This is more prevalent for larger particle sizes as they are more subject to deformation (Ref. 9). It was also mentioned in the previous section that the HSI instruments had a digital resolution of 3.73 μm/pixel. Under practical conditions like those in PSL, the HSI instruments used for this test had lower measurement limits of approximately 15 μm, ideally, but roll off generally occurred around 15 to 20 μm.

To take advantage of the measurement capabilities of both instruments and obtain a PSD across the full particle size spectrum, the PDI data was used to define the PSD below 20 μm, and the HSI data was used to define the PSD above 20 μm, and the two distributions were merged together, as described below. The acceptance criteria for the PDI data was limited to a very narrow band of approximately 2° along the calibrated phase shift-size relationship (Refs. 9 and 15). To account for rejected scattering events, the counts in each PDI histogram bin were corrected by multiplying the accepted counts by the ratio of the total rejected counts to the total accepted counts. The data from the HSI were fitted with Generalized Extreme Value (GEV) distributions prior to joining the PDI and HSI distributions. The GEV distribution is a probability density function (PDF) that was applied to account for the low counting statistics near the higher end of the size spectrum of the HSI data, as previously mentioned. Figure 2 shows the Number Density (ND) distribution with the experimental data from the PDI and HSI for Escort Number 226, without the application of the GEV distribution, and the combined ND distribution that resulted from the processing described above. Figure 2 demonstrates that the PDI captures the lower end of the spectrum where the HSI rolls off quickly, and the use of the GEV distribution smooths the PSD at the upper end of the spectrum, creating a distribution that captures the data from both instruments.

Table 3 provides the Total Water Content (TWC) and selected cumulative volume distribution values from the PSD. This data was generated applying the methodology described above. Figure 3 shows the $d_{v0.50}$ data and trends for the pressure sweeps for p_{AIR} values of 20 and 30 psi. Neglecting the potential outlying point at $\Delta p = 80$ psi in the $p_{AIR} = 20$ psi, $T_{WB} > 0$ °F series, the data for all three sets are captured well by 2nd order polynomials, which are shown by the solid lines. These appear to be predictable trends as a function of p_{AIR} and Δp. The dashed line shows the 2nd order polynomial for the $p_{AIR} = 20$ psi, $T_{WB} > 0$ °F series when the $\Delta p = 80$ psi point is included in trend analysis. There is no indication in the data from the Artium instruments or the facility that explains this apparent outlier. The trends for the data with $T_{WB} > 0$ °F are both concave, while the trend for the $p_{AIR} = 20$ psi, $T_{WB} < 0$ °F is convex, which is the characteristic typically expected for particle size data of this nature. It is worth noting that the u_{SI} for the $p_{AIR} = 20$ psi, $T_{WB} < 0$ °F series was reduced by approximately 8 m/s, introducing possible air speed effects. Review of Table 1 demonstrates that there was insufficient data to adequately investigate the effect of u_{SI} on PSD for ice crystal conditions. However, there was sufficient data to examine the effects of thermodynamic conditions on the PSD. Referring to Tables 1 and 3, the data from the ice crystal portion of the test shows that reductions in T_{WB}, which is a function of the plenum pressure, P_{PL}, the plenum temperature, T_{PL}, and the relative humidity, ϕ_{PL}, result in moving the distributions towards the lower end of the size spectrum, thus reducing $d_{v0.50}$. However, this shift was typically on the order of 1 μm for a 10 °F reduction during this test. This can be observed specifically in comparison between the two $p_{AIR} = 20$ psi series with either $T_{WB} < 0$ °F or $T_{WB} > 0$ °F. Additional data is necessary to determine if this a repeatable behavior or attributable to the combination of facility and measurement uncertainties. Further testing that includes systematic repeat measurements is necessary to solidify these conclusions.

Finally, Figure 4 shows the TWC comparison between the centerline experimental and trend data from the IKP2 and data from the Artium instruments. The two sets of data tend to agree to within ±20 percent, which is enveloped by the dotted lines in Figure 4. There are a few apparent exceptions to this, which are typically observed for test conditions that utilized the Standard (STD) nozzle set.

Supercooled Liquid Water Test Conditions

Only the data from the PDI was used to determine the PSD for the supercooled liquid water test conditions. This was done because many of the conditions during the supercooled liquid water portion of the test had distributions principally below the lower measurement limit of the HSI, the measurement range of the PDI encompassed the entire size spectrum, and there were no indications from the PDI phase shift-size relationship data of the presence of ice crystals (Ref. 9).

Table 4 shows TWC and cumulative volume distribution values for each test condition. Figure 5 shows the $d_{v0.50}$ data and trends for the pressure sweeps for p_{AIR} values of 15 and 20 psi. Similar to the ice crystal pressure sweeps, the data for both series are captured well by 2nd order polynomials, which are shown by the solid lines. Again, these appear to be predictable trends as a function of p_{AIR} and Δp. Table 2 shows that the majority of the remaining test conditions were points with either p_{AIR} = 15 psi and Δp = 45 psi or p_{AIR} = 20 psi and Δp = 20 psi, with varying u_{SI} and thermodynamic conditions. The data does not indicate any significant sensitivities to variation of these parameters. Examining the distribution values and the u_{SI} values for Escort Numbers 283, 286 and 287 in Tables 2 and 4, respectively, demonstrates this observation. For a total increase of u_{SI} by a factor of almost two, the change in each distribution value is relatively flat, only varying by approximately ±1 μm, except for the 3 μm drop in $d_{v0.90}$ seen in 283. Similarly, examining Escort Numbers 270, 275, 282, 284, 285 and 288 in Tables 2 and 4, the variation of thermodynamic conditions does not indicate a discernable trend. The lower end of the distributions, including $d_{v0.10}$, $d_{v0.25}$ and $d_{v0.50}$ for these cases remain fairly constant, while the upper end of the distributions, including $d_{v0.75}$ and $d_{v0.90}$, noticeably shift. In the case of $d_{v0.90}$, the shift is as much as 5 μm. However, using the previous finding that changes in u_{SI} will not have significant effects on the distribution in the supercooled liquid water regime, a reasonable trend relating the changes in both $d_{v0.75}$ and $d_{v0.90}$ and T_{WB} cannot be developed. Again, additional data is necessary to determine if this is attributable to the combination of facility and measurement uncertainties. Further testing that includes systematic repeat measurements is necessary to solidify these conclusions.

Figure 4 shows the LWC comparison between the centerline experimental and trend data from the MW, the experimental data from the MW at a radius of 20 cm from the centerline, and the data from the Artium instruments. The MW data at a radius of 20 cm was acquired concurrent with the Artium PSD data per the test conditions defined in Table 2. This data set averages the last 30 sec of measurements from the MW total water sensor for the spray, and shows good agreement with the LWC obtained by the Artium instruments, where the majority of the LWC values are within ±20 percent. The centerline experimental and trend data from the MW do not demonstrate the same level of agreement, where the data appears to have a slope greater than the 1:1 line and is slightly shifted in the positive direction of the horizontal axis.

Summary and Conclusions

NASA completed the 2017 PSL Cloud Calibration Test, where the Artium Technologies, Inc. PDI-MOD, HSI-MOD, and HSI-FPDR were used to characterize the PSD under ice crystal and supercooled liquid icing conditions. The available PSD data from the Artium instruments indicate predictable trends, where the PSD is primarily a function of the nozzle air and water pressure settings for both ice crystal and supercooled liquid icing conditions. Additionally, the water content measurements from the Artium instruments are generally in good agreement with the IKP2 and MW instruments in both sets of conditions. Reductions in the T_{WB} appears to shift the PSD towards the lower end of the size spectrum for the ice crystal conditions, but the data does not indicate that the effect is significant.

Insufficient data was available to demonstrate the effect of air speed for the ice crystal conditions. In the supercooled liquid water conditions, the data indicates u_{SI} does not have significant effects on the PSD. There is variation in the upper end of the size spectrum with changes in thermodynamic conditions for the supercooled liquid water conditions, however, there does not appear to be a discernable trend to these changes. These may be related to the combination of facility and measurement uncertainties. Further testing that includes systematic repeat measurements is necessary to solidify these conclusions.

References

1. Mason, J.G., Strapp, J.W., and Chow, P., "The Ice Particle Threat to Engines in Flight," *44th AIAA Aerospace Sciences Meeting and Exhibit*, AIAA-2006-206, 2006.
2. Oliver, M.J., "Validation Ice Crystal Icing Engine Test in the Propulsion Systems Laboratory at NASA Glenn Research Center," *6th AIAA Atmospheric and Space Environments Conference*, AIAA-2014-2898, 2014.
3. Goodwin, R.V., and Dischinger, D.G., "Turbofan Ice Crystal Rollback Investigation and Preparations Leading to Inaugural Ice Crystal Engine Test at NASA PSL-3 Facility," *6th AIAA Atmospheric and Space Environments Conference*, AIAA-2014-2895, 2014.
4. Tsao, J.C., Struk, P.M., and Oliver, M.J., "Possible Mechanisms for Turbofan Engine Ice Crystal Icing at High Altitude," *6th AIAA Atmospheric and Space Environments Conference*, AIAA-2014-3044, 2014.
5. Flegel, A.B., Oliver, M.J., "Preliminary Results from a Heavily Instrumented Engine Ice Crystal Icing Test in a Ground Based Altitude Test Facility," *8th AIAA Atmospheric and Space Environments Conference*, AIAA-2016-3894, 2016.
6. Struk, P.M., Taso, J.C., and Bartkus, T.P., "Plans and Preliminary Results of Fundamnental Studies of Ice Crystal Icing Physics in the NASA Propulsion Systems Laboratory," *8th AIAA Atmospheric and Space Environments Conference*, AIAA-2016-3738, 2016.
7. Struk, P.M., Ratvasky, T.P., Bencic, T.J., Van Zante, J.F., King, M.C., Taso, J.C., and Bartkus, T.P., "An Initial Study of the Fundamentals of Ice Crystal Icing Physics in the NASA Propulsion Systems Laboratory," *9th AIAA Atmospheric and Space Environments Conference*, American Institute of Aeronautics and Astronautics, AIAA-2017-4242, 2017.
8. Van Zante, J.F., Bencic, T.J., Ratvasky, T.P., "NASA Glenn Propulsion Systems Lab Ice Crystal Cloud Characterization Update 2015," *8th AIAA Atmospheric and Space Environments Conference*, AIAA-2016-3897, 2016.
9. King, M.C., Bachalo, W.D., and Kurek, A., "Particle Size Measurements from the first Fundamentals of Ice Crystal Icing Physics Test in the NASA Propulsion Systems Laboratory," *9th AIAA Atmospheric and Space Environments Conference*, AIAA-2017-4244, 2017.
10. Davison, C.R., Ratvasky, T.P., and Lilie, L.E., "Naturally Aspirating Isokinetic Total Water Content Probe: Wind Tunnel Test Results and Design Modifications," *SAE 2011 International Conference on Aircraft and Engine Icing and Ground Deicing*, 2011-38-0036, 2011.
11. Bencic, T.J., Fagan, A., Van Zante, J.F., Kirkegaard, J.P., Rohler, D.P., Maniyedath, A., and Izen, S.H., "Advanced Optical Diagnostics for Ice Crystal Cloud Measurements in the NASA Glenn Propulsion Systems Laboratory," *5th AIAA Atmospheric and Space Environments Conference*, AIAA-2013-2678, 2013.
12. Struk, P.M., Tsao, J.C., and Bartkus, T.P., "Plans and Preliminary Results of Fundamental Studies of Ice Crystal Icing Physics in the NASA Propulsion Systems Laboratory," *8th AIAA Atmospheric and Space Environments Conference*, AIAA-2016-3738, 2016.
13. Van Zante, J.F., Ratvasky, T.P., Bencic, T.J., Timko, E.N., and Challis, C.C., "Update on the NASA Glenn Propulsion Systems Lab Icing and Ice Crystal Cloud Characterization (2017)," *10th AIAA Atmospheric and Space Environments Conference*, American Institute of Aeronautics and Astronautics, Atlanta, GA (to be submitted for publication).

14. Agui, J.H., Bartkus, T.P., and Struk, P.M., "Total Temperature Measurements Using a Rearward Facing Probe in Supercooled Liquid Droplets and Ice Crystal Clouds," *10th AIAA Atmospheric and Space Environments Conference*, American Institute of Aeronautics and Astronautics, Atlanta, GA (to be submitted for publication).

15. Albrecht, H.-E., Damaschke, N., Borys, M., and Tropea, C., *Laser Doppler and Phase Doppler Measurement Techniques*, Springer-Verlag, Berlin, 2003.

16. King, M.C., Bachalo, W.D., Bell, D., and King-Steen, L.E., "Weber Number Tests in the NASA Icing Research Tunnel," *10th AIAA Atmospheric and Space Environments Conference*, American Institute of Aeronautics and Astronautics, Atlanta, GA (to be submitted for publication).

TABLE 1.—ICE CRYSTAL TEST CONDITIONS

Escort no.	Nozzle type	Nozzle quantity	p_{AIR}	Δp	u_{SI}	p_{PL}	T_{PL}	ϕ_{PL}	p_{SI}	T_{WB}[a]
---	---	---	psi	psi	m/s	psi	°F	%	psi	°F
223	MOD	36	20	20	149	3.3	26	45	2.8	7.5
224	MOD	84	20	20	147	3.3	26	47	2.8	7.8
225	MOD	84	20	20	148	3.3	26	46	2.8	8.1
226	MOD	84	20	30	147	3.3	26	46	2.8	8.3
228	MOD	84	20	40	148	3.3	26	47	2.8	7.9
229	MOD	84	20	50	147	3.3	26	47	2.8	7.9
230	MOD	84	20	60	147	3.3	26	46	2.8	7.8
231	MOD	84	20	80	147	3.3	26	47	2.8	7.8
232	MOD	84	20	100	147	3.3	26	46	2.8	7.9
233	MOD	84	30	20	147	3.3	26	46	2.8	8.3
234	MOD	84	30	40	147	3.3	26	47	2.8	8.2
235	MOD	84	30	60	147	3.3	26	46	2.8	7.8
236	MOD	84	30	80	147	3.3	26	47	2.8	7.9
237	STD	43	40	40	147	3.3	26	46	2.8	7.7
238	STD	77	40	40	146	3.3	27	46	2.9	7.9
239	STD	37	40	40	148	3.3	26	46	2.8	7.5
240	STD	69	40	40	147	3.3	26	46	2.8	7.8
241	STD	69	40	50	147	3.3	26	46	2.8	7.8
242	STD	69	40	60	147	3.3	26	46	2.9	7.7
243	STD	69	30	40	147	3.3	26	46	2.8	7.5
244	STD	69	30	50	147	3.3	27	44	2.8	7.9
245	STD	69	30	60	147	3.3	27	44	2.8	8.1
246	MOD	36	20	10	139	3.1	14	46	2.7	−3.0
247	MOD	36	20	20	139	3.1	14	44	2.7	−2.6
248	MOD	84	20	30	141	3.1	14	45	2.7	−2.7
249	MOD	84	20	40	140	3.1	15	45	2.7	−2.6
250	MOD	84	20	50	141	3.1	14	46	2.7	−2.9
251	MOD	84	20	60	140	3.1	14	46	2.7	−2.8
252	MOD	84	20	80	139	3.1	11	45	2.7	−4.4
253	MOD	84	30	60	140	3.1	15	44	2.7	−2.8
254	MOD	84	20	60	139	4.1	26	43	3.7	6.8
255	MOD	84	20	45	142	4.1	25	44	3.6	7.3
256	MOD	84	20	45	141	5.3	25	45	4.6	6.5

[a]Values based on conditions in the plenum

TABLE 2.—SUPERCOOLED LIQUID WATER TEST CONDITIONS

Escort no.	Nozzle type	Nozzle quantity	p_{AIR}	Δp	u_{SI}	p_{PL}	T_{PL}	ϕ_{PL}	p_{SI}	T_{WB}[a]
---	---	---	psi	psi	m/s	psi	°F	%	psi	°F
265	MOD	36	16	40	61	12	27	44	12	19
266	MOD	36	15	45	59	12	26	47	12	19
267	MOD	36	15	30	61	12	26	46	12	19
268	MOD	36	20	5	61	12	27	46	12	19
269	MOD	36	20	10	61	12	27	45	12	19
270	MOD	36	20	20	61	12	27	46	12	19
271	MOD	36	20	40	61	12	26	47	12	19
272	MOD	26	10	5	29	12	25	43	12	19
273	MOD	26	10	10	29	12	24	46	12	19
274	MOD	26	10	10	74	10	22	45	9	13
275	MOD	36	20	20	74	10	22	45	9	13
276	MOD	36	20	40	74	10	22	45	9	13
277	MOD	26	5	20	27	12	23	44	12	17
278	MOD	84	5	20	44	12	21	47	12	15
279	MOD	36	15	15	43	12	21	47	12	16
280	MOD	36	20	40	43	12	20	46	12	15
281	MOD	36	15	45	60	12	23	45	12	16
282	MOD	36	20	20	73	13	11	48	12	5
283	MOD	36	15	40	49	10	13	46	10	7
284	MOD	36	20	20	49	10	12	45	10	7
285	MOD	36	20	20	70	10	15	44	9	8
286	MOD	36	15	40	69	10	15	45	9	7
287	MOD	36	15	40	83	10	16	44	9	7
288	MOD	36	20	20	83	10	16	46	9	7
289	MOD	36	15	40	48	10	15	46	10	10

[a]Values based on conditions in the plenum

TABLE 3.—ICE CRYSTAL PARTICLE SIZE RESULTS

Escort no.	TWC	$d_{v0.10}$	$d_{v0.25}$	$d_{v0.50}$	$d_{v0.75}$	$d_{v0.90}$
---	g/m^3	μm	μm	μm	μm	μm
223	1.0	9	12	17	23	31
224	1.4	10	14	21	29	37
225	1.6	10	13	20	28	36
226	1.9	11	15	22	31	40
228	2.3	11	16	24	34	45
229	2.7	12	18	26	38	52
230	2.6	14	19	28	40	55
231	3.1	12	18	27	42	61
232	3.8	13	20	31	49	74
233	1.5	10	13	18	24	30
234	1.9	11	15	21	29	37
235	2.0	12	16	23	32	42
236	3.0	11	16	24	35	47
237	3.1	13	19	29	44	62
238	12	17	25	38	57	77
239	3.5	12	17	28	43	64
240	4.7	13	20	30	46	64
241	6.0	14	21	34	56	82
242	9.2	15	22	37	62	90
243	6.2	13	18	32	55	86
244	11	16	26	45	81	122
245	11	16	25	43	75	115
246	0.4	8	12	18	25	31
247	0.5	10	14	21	28	36
248	2.1	11	15	22	30	39
249	2.5	11	16	23	32	43
250	3.0	12	17	25	36	50
251	3.0	13	19	27	39	55
252	4.1	11	17	27	41	59
253	2.3	12	17	23	32	42
254	2.8	11	16	25	38	53
255	2.2	10	14	20	30	40
256	2.9	11	15	21	31	43

TABLE 4.—SUPERCOOLED LIQUID WATER PARTICLE SIZE RESULTS

| Escort no.	LWC	$d_{v0.10}$	$d_{v0.25}$	$d_{v0.50}$	$d_{v0.75}$	$d_{v0.90}$
---	g/m^3	μm	μm	μm	μm	μm
265	1.1	11	16	25	40	60
266	1.5	11	17	27	43	64
267	1.2	8	13	22	33	44
268	0.1	4	6	9	12	14
269	0.1	5	8	11	14	18
270	0.5	6	9	13	18	24
271	1.8	9	13	20	31	45
272	0.2	7	9	13	18	24
273	0.4	8	11	17	25	34
274	0.2	7	10	15	22	30
275	0.3	6	8	12	17	24
276	1.3	8	12	19	30	44
277	1.4	16	25	42	71	105
278	6.3	15	24	42	71	105
279	1.0	8	11	18	25	32
280	1.6	8	11	18	27	40
281	1.7	11	17	28	44	67
282	0.7	6	8	13	19	28
283	1.8	10	16	26	38	53
284	0.7	6	9	12	17	22
285	0.5	6	10	14	21	29
286	1.5	11	16	26	40	57
287	1.3	11	17	27	40	57
288	0.4	6	8	12	17	24
289	2.0	9	15	24	37	52
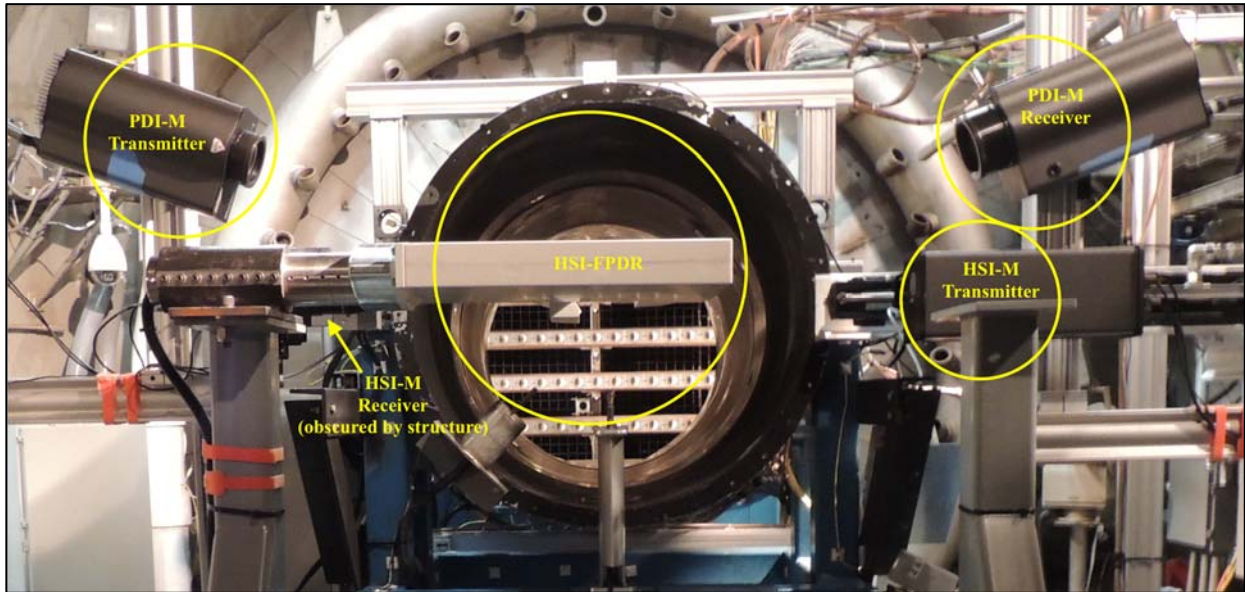
Figure 1.—PSL Cloud Calibration Test PSD Configuration setup, showing the Artium Technologies, Inc. PDI and HSI instruments focused approximately at the centerline of the duct.
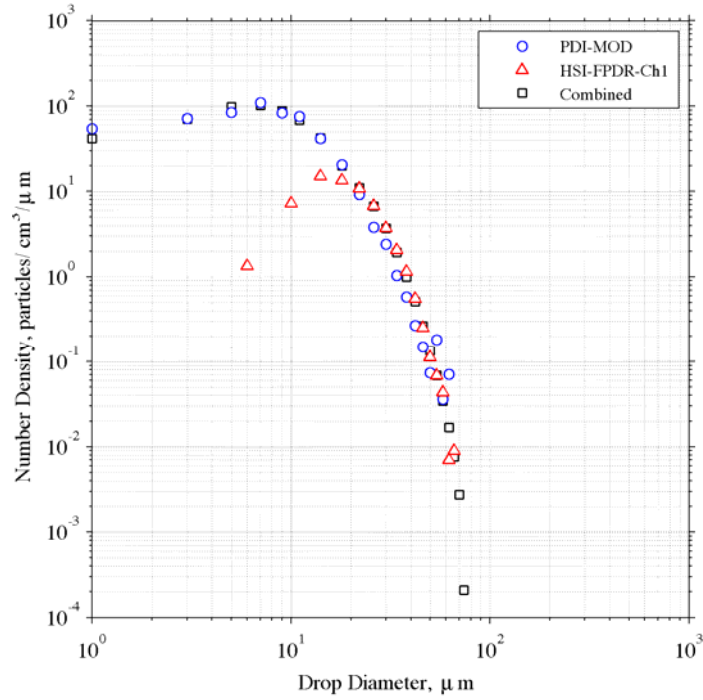
Figure 2.—Number density distributions from of the PDI and HSI, and the combined distribution using a GEV PDF for Test Condition 226.
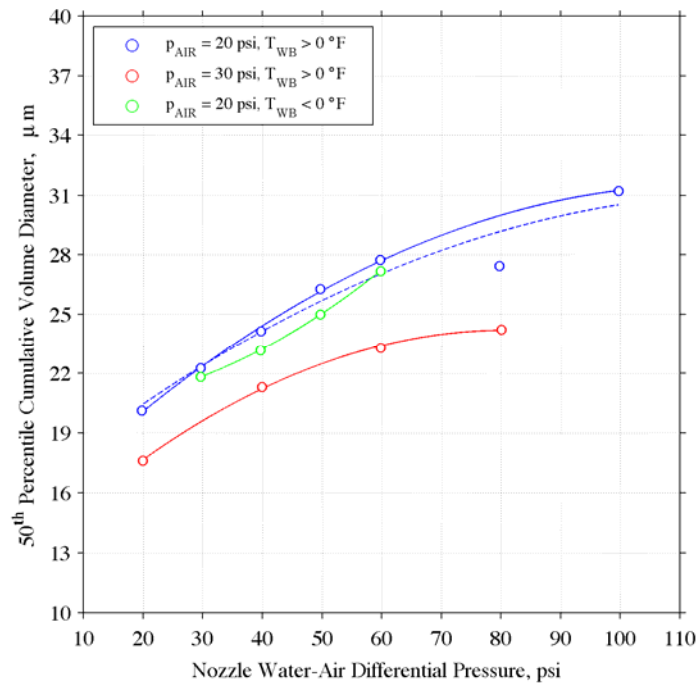

Figure 3.—The 50th Percentile Cumulative Volume Diameter as a function of nozzle water-air differential pressure sweeps for p_{AIR} = 20 and 30 psi and varying T_{WB} from the ice crystal test conditions with trends.
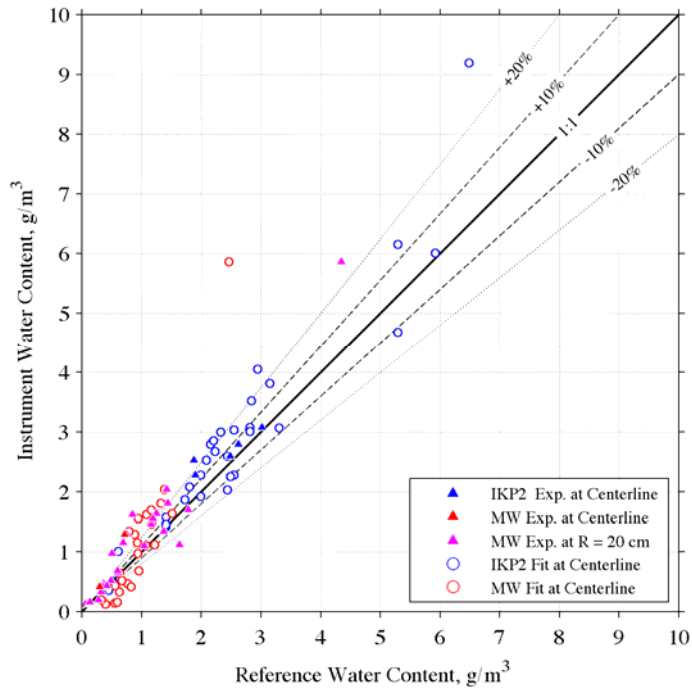
Figure 4.—Water content comparison summary, between IKP2 and MW data (horizontal axis) and the PDI and HSI data (vertical axis).
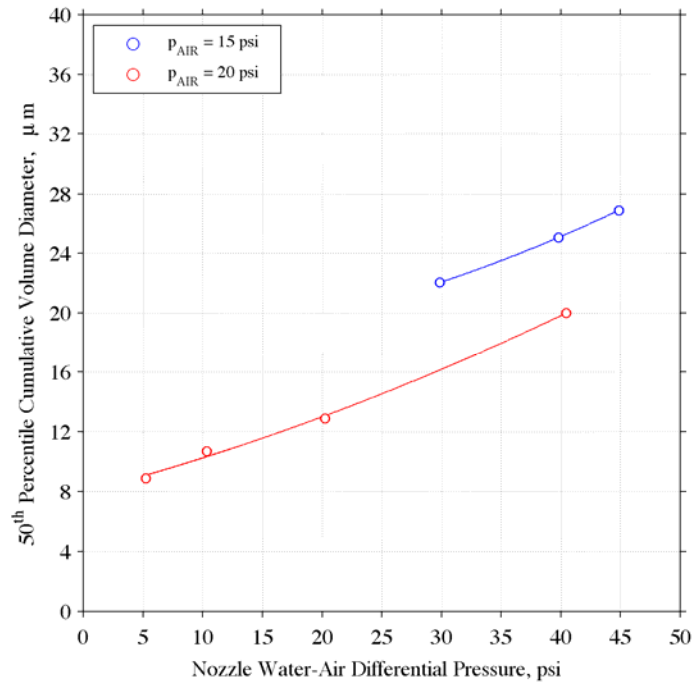

Figure 5.—The 50th Percentile Cumulative Volume Diameter as a function of nozzle water-air differential pressure sweeps for p_{AIR} = 15 and 20 psi from the supercooled liquid water test conditions.